Chemical reactivity of lithium difluorophosphate as electrolyte additive in LiNi0.6Co0.2Mn0.2O2/graphite cells

Ana Cristina Martinez, Sebastien Rigaud, Sylvie Grugeon, Pierre Tran-Van, Michel Armand, Dominique Cailleu, Serge Pilard, Stéphane Laruelle

Chemical reactivity of lithium difluorophosphate as electrolyte additive in $LiNi_{0.6}Co_{0.2}Mn_{0.2}O_2$/graphite cells

Ana Cristina Martinez[a,b,c], Sébastien Rigaud[d], Sylvie Grugeon[a,b], Pierre Tran-Van[c], Michel Armand[e], Dominique Cailleu[d], Serge Pilard[d], Stephane Laruelle[a,b*]

[a]*Laboratoire de Réactivité et Chimie des Solides, CNRS UMR 7314, Université de Picardie Jules Verne, 33 rue Saint Leu, 80039 Amiens, France*
[b]*Réseau sur le Stockage Electrochimique de l'Energie, CNRS RS2E FR3459, France*
[c]*Renault, DEA-IREB, Technocentre, 1 avenue du Golf, 78288 Guyancourt, France*
[d]*Plate-Forme Analytique, Université de Picardie Jules Verne, 33 rue Saint Leu, 80039 Amiens, France*
[e]*Centre for Cooperative Research on Alternative Energies (CIC energiGUNE), Basque Research and Technology Alliance (BRTA), Alava Technology Park, Albert Einstein 48, 01510, Vitoria-Gasteiz, Spain*

[*]*corresponding author: stephane.laruelle@u-picardie.fr*
Tel: +33 322825779

Keywords: lithium difluorophosphate, lithium salt, LC-MS, electrolyte additive, Li-ion battery

Abstract

From the literature overview, lithium difluorophosphate salt, $LiPO_2F_2$, is considered a powerful electrolyte additive capable of enhancing lithium-ion batteries' capacity retention. Lower cell impedance associated with SEI and/or CEI layers composition and texture modifications had been widely demonstrated, but without providing clear mechanisms. This paper sheds light on the reactivity of $LiPO_2F_2$ by combining electrochemical measurements and analyses of electrolyte degradation products at the interphases and in the electrolytes by means of infrared and mass spectrometry techniques. Fluorine substitution reaction by electrochemically formed anions leads to a mitigation of electrolyte solvents degradation and to the enrichment of the SEI layer with LiF and lithium organofluorophosphates. Furthermore, a discussion on the composition of the CEI layer that enables the prevention of the transition metals dissolution from positive electrode layered oxides materials is also presented.

1. Introduction

Accelerating zero-emission mobility is urgently required in an attempt to stabilize global temperature near its current level and improve air quality. This challenging objective involves the deployment of electric vehicles with high-performance, fast-charging, safe, inexpensive, and long-lasting battery technology[1–3]. Currently, only Li-ion batteries offer acceptable but still improvable features[4].

Intrinsically, the cycling potential range of the current high-energy density Li-ion batteries exceeds the electrolyte electrochemical stability window, which makes imperative the formation of an electronically insulating and lithium cation conducting passivation layer, called solid electrolyte interphase (SEI)[5], at the negative electrode material surface. As a consequence, long-lasting and safe battery functioning mostly relies on the ability of this layer to mitigate solvents electrochemical reduction while subjected to ageing processes such as material cracks due to abuse thermal conditions or expansion/contraction phenomenon upon lithiation/delithiation processes. SEI reinforcing electrolyte additives remain one of the most effective and economical ways to meet these expectations. Generally, a mix of neutral molecules such as vinylene carbonate (VC)[6], fluoroethylene carbonate (FEC)[7], 1,3-propane sultone (PS)[8], succinonitrile (SN)[9]… able to reduce before carbonate solvents and to form passivating precipitated lithium salt or polymers at the outermost surface of the negative active material, is generally added in the electrolyte, in a quantity depending on the material surface area to protect.

Several electrolyte degradation reactions may also take place on the surface of cathode materials; i) the electrolyte carbonate solvents undergo electrochemical oxidation at high potential[10], ii) the delithiation-induced structural degradation of Ni-rich layered metal oxides [11] cathodes ($LiNi_{1-x-y}Mn_xCo_yO_2$ also called NMC) is concomitant with O^{2-} oxidation in oxide lattices, and subsequent singlet O_2 gas evolution[10]. As a deleterious impact, this released reactive species can easily oxidize the electrolyte, resulting in the formation of water and gaseous products such as CO_2 and CO in the battery cell, and iii) the water, as impurity and solvents oxidation by-product, reacts with $LiPF_6$, releasing LiF, POF_3, PO_4^{3-} and the HF acid[12,13]. Hydrofluoric acid[12,14,15] but also NMC surface structural evolutions[16] are responsible for the dissolution of transition metals (TMs) from cathodes. This dissolution was evidenced by the use of inductively coupled plasma (ICP) technique[15–17] or operando X-ray absorption spectroscopy[18]. TMs were found to dissolve nearly stoichiometrically at potentials > 4.3 and 4.6 V for NMC 111[15] and 622[19], respectively, and to display low oxidation

states[16,18]. The mechanism(s) of TMs dissolution seems quite complex and still in debate[16].

These adverse reactions make it essential the protection of the cathode material surface by coating[20] or building a passivation layer (called cathode electrolyte interface layer - CEI layer) with electrolyte additives[21,22] to mitigate the decrease in capacity retention.

From 2015, interest in a lithium salt-type electrolyte additive, the lithium difluorophosphate, $LiPO_2F_2$ (LDFP) as an electrolyte additive has increased due to its presumed ability to build reinforced organic-inorganic hybrid interphases on the positive and negative electrodes. Studies have shown many positive outcomes in a variety of positive and negative electrode chemistries in half or full cells, with NMC cathode materials being among the most common. Under different cycling conditions, temperatures between -25°C and 55°C and weight content usually between 0.5 and 3 wt.% (a maximum amount due to its limited solubility[23]), LDFP can:

- decrease positive electrode[24–30], negative electrode[25,31,32] or full cell[25,28,29,33–35] impedances
- prevent lithium plating[25] and decrease TM cation dissolution[33,36]
- decrease gas production after storage at high temperature[25,32,37]
- impede surface transformations from layered to rock salt structure in NMC 622[38] and
- improve capacity retention after at least 100 cycles at different C-rate from C/3 to 2C, in half cells or pouch cells with upper cut-off voltages as high as 4.5 V *vs*. Li/Li^+[24,32,33,39–42].

A great deal of research has been devoted to highlighting the physicochemical or electrochemical origin of these improved properties. Consumption of this additive during the formation step was proven through electrolyte NMR analysis[32] and all studies reported an impact of LDFP at the negative and/or positive electrodes through the observation of a thinner and denser SEI[39] and/or CEI[26,28,29] layer by means of transmission electron microscopy (TEM). F1s and P2p XPS spectra analysis usually revealed a higher amount of fluorophosphate species (Li_xPF_y and $Li_xPF_yO_z$)[24,26,31,33,34,43,44] and/or LiF[26,34,44,45] whose origin is still debated. Only one study reported the use of Infrared spectroscopy [28]. With the appearance of peaks at 1317 and 962 cm^{-1}, the authors explain that LiDFP, when added to 1 M LiODFB in EC/DMC electrolyte, is involved in the interfacial reaction of the $LiNi_{0.5}Mn_{1.5}O_4$ surface (CEI). Apart from one study[31] in which a peak of the SEI formation was observed at a higher potential in the presence of LDFP and attributed to its reduction, most of the authors agreed to say that LDFP does not reduce. Regarding its oxidation, the results are not as

conclusive. In a few experiments, an oxidation peak was shown either at low or high potential, in the 2.7 - 4.6V range[26,46]. This result would corroborate the theoretical DFT calculation suggesting it is likely to oxidize at a lower potential than carbonate solvents; Chen et al.[24] calculated that the oxidation of LDFP would occur around 5.9 V, before the calculated oxidation of EC at 6.97 V or EMC at 6.78 V[33]. By contrast, other authors propose that LDFP simply precipitates at the interphases. According to G. Yang et al.[43], it would promote the migration of lithium ions to electrodes through the formation of ion-triplets or -doublets, $Li_xPO_2F_2$ (x = 2 or 3) as a lithium carrier, and deposit on the active material surface after charge transfer processes. In light of this bibliographic work, none of the hypotheses present a concrete and sufficiently grounded explanation of what occurs to the interfaces when LDFP is used.

Furthermore, Qian et al.[45] in 2019 analyzed the electrolyte after the initial charging process through gas chromatography mass spectrometry (GC-MS) and liquid chromatography mass spectrometry (LC-MS). Surprisingly, the authors did not reveal any of the cycling degradation compounds whose formation is initiated by electrochemical reduction processes. Although these results are remarkable, the question still arises as to whether this effect originates in physical (efficient passivating SEI layer preventing parasitic reactions) or chemical (initiator trapping) processes.

Motivated by our previous study demonstrating that this appealing additive, LDFP, could also be produced at the positive electrode as a product of the chemical reaction between NMC surface species such as Li_2CO_3, Li_2O, Li_2SO_4[47] and coating components such as Al_2O_3[48] with the lithium salt, $LiPF_6$, further work to better understand its reactivity as electrolyte additive in Li-ion cells was undertaken. Beforehand, its influence on the ionic conductivity and the electrolyte electrochemical stability was studied. Afterward, decomposition products present in graphite (SEI) and NMC622 (CEI) material surface layers and in the electrolyte were analyzed by means of Fourier Transform-Infrared (FT-IR) spectroscopy and ultra-high-performance liquid chromatography-hyphenated electrospray ionization – high-resolution mass spectrometry (UHPLC-ESI-HRMS) techniques, respectively. Based on the results of this study and the literature, we provide further explanations for the beneficial impact of LDFP upon cycling.

2. Experimental

2.1. Ionic conductivity and viscosity measurements and cyclic voltammetry

Temperature-dependent ionic conductivities of the electrolyte solutions were measured in sealed vials, using a CDC749 (Radiometer analytical) cell connected to an MTZ-35 frequency response analyzer (Biologic). Thanks to a Julabo FP50 refrigerated/heating circulator, the temperature was maintained for at least 30 min at each temperature before the measurements were performed. The reported values are an average of three measurements with a relative standard error of less than 5%. Same measurements were carried out with electrolyte solution impregnated in a 25µm thick microporous (55%) polypropylene separator (Celgard 2500) sandwiched between two copper electrodes (4 and 4.4 cm^2), in a pouch bag. The viscosity of the electrolytes was measured using a Brookfield DV-II+Pro viscosimeter connected to a cryostat at 25°C. Cyclic voltammetry (CV) measurements were conducted on a VMP-3 potentiostat/galvanostat (Biologic) by using Pt as working and counter electrode, and Li as reference electrode, in the 0.05-6 V range, at a scanning rate of 30 mV s^{-1}.

2.2. Half-cells cycling and interphase layers analysis using FT-IR spectroscopy

The Swagelok-type half-cells were assembled in an argon-filled glove-box using 10 mg composite powder containing 90 wt.% graphite (Timrex E-SLS30, Ymerys) or $LiNi_{0.6}Mn_{0.2}Co_{0.2}O_2$ (NMC622, Umicore) and 10 wt.% carbon black (C45, Ymerys) as working electrode, a Whatman GF/D borosilicate glass fibre separator impregnated with 150 µL of electrolyte and a lithium metal foil (Sigma-Aldrich). The electrolyte contained 1M $LiPF_6$ in a 1:1:1 vol. mixture of EC/DEC/EMC (99.9%, H_2O < 20 ppm, Solvionic) with or without 0.2M lithium difluorophosphate (Guangzhou Tinci Materials Technology Co., Ltd). Once assembled, the cells were subjected to one cycle at C/20 (considering x=1 in Li_xC_6 and $Li_xNi_{0.6}Mn_{0.2}Co_{0.2}O_2$) between 0.005-1.5 V and 4.3-2.8V *vs.* Li^o/Li^+ respectively.

After cycling, the cells were opened in the argon-filled glove-box, the recovered Li_0C_6 powders were rinsed three times with DMC to eliminate residual traces of solvents and $LiPF_6$ salt, and subsequently dried in the antechamber. FT-IR spectra were recorded by means of a Nicolet iS20 spectrometer. The synthesized powders were analyzed in transmission mode through KBr pellets. The powder-containing pellet mounted on the holder was prepared in the glove-box (pressure of compaction of 8 tons) and put in a plastic bag which was opened in the N_2-purged sample chamber of the FT-IR system.

2.3. Pouch cells prototype fabrication and cycling

Both single side coated electrodes were laboratory-made. Positive electrodes (4 cm^2) prepared in a dry room (dew point of -58°C) were composed of $LiNi_{0.6}Mn_{0.2}Co_{0.2}O_2$ active material (~19

mg.cm^{-2}), carbon black C45 and PVdF binder (Sigma Aldrich) in a 90/6/4 weight ratio. Negative electrodes (4.84 cm^2) were prepared under ambient air from a slurry containing graphite (~9 mg.cm^{-2}), C45, CMC and Triton-X100 (Sigma Aldrich) in a 91.6/4/4/0.4 weight ratio. Both electrodes were dried at 60°C then calendered to obtain 30-35% porosity. The separator was a porous polypropylene membrane (Celgard 2500). Pouch cells with a capacity of around 14 mAh at 55°C were prepared in the dry room. They were vacuum-dried overnight at 80 ºC before being filled with electrolyte (80 µL). Cells were stored in the oven at 25°C for 5h then cycled at 55°C in galvanostatic mode at C/10 (considering x=1 in $Li_xNi_{0.6}Mn_{0.2}Co_{0.2}O_2$) between 2.8 and 4.3 V with a rest time of 10 min. between each charge and discharge sweep.

2.4. Electrolyte recovery from pouch cell prototype and UHPLC-ESI-HRMS analysis

After cycling, the cells were introduced into the glove box. After opening and dismantling the cell, the separator was put, folded, in a small glass flask and 0.4 mL of acetonitrile (HPLC-MS grade purchased from Biosolve) was added. Vortex stirring for 3 min. was applied to ensure all species from the separator were dissolved. The resulting liquid was diluted 2000 times with acetonitrile of the same grade for UHPLC-ESI-HRMS analysis. In order to verify that the hereafter described experimental protocol did not produce the degradation products identified in this study, the electrolyte alone was first tested.

Electrospray high-resolution mass spectrometry experiments (ESI-HRMS) were performed on a hybrid quadrupole time-of-flight instrument (SYNAPT G2-Si, Waters), hyphenated with a UHPLC system (ACQUITY UPLC H-Class). This instrument has an electrospray (ESI) ionization source (Z-spray) and an additional sprayer (Lock Spray) for the reference compound. UHPLC was performed using an ACQUITY UPLC HSS T3 (100×2.1 mm, 1.8 µm) column from Waters, maintained at 40°C. The elution was performed using a 0.5 mL/min mobile phase gradient of water (A) and acetonitrile (B) both containing 0.1 % formic acid. The gradient used was : (A:B): 100:0 (t = 0 min), 100:0 (t = 2 min), 40:60 (t = 8 min), 40:60 (t = 9 min), 20:80 (t = 11 min), 20:80 (t = 12 min), 100:0 (t = 13 min), 100:0 (t = 17 min). The ESI source was operated in the positive ion mode using a capillary voltage of 3 kV under the following conditions: cone voltage, 40 V; source offset, 40 V; source temperature, 120°C; desolvation gas temperature, 450°C; desolvation gas flow, 800 L/h, and cone gas flow, 50 L/h. Nitrogen (> 99.5%) was employed as the desolvation and cone gas. Mass calibration was carried out using a sodium formate solution (10 mM NaOH in isopropanol/water/formic acid 49.9:49.9:0.2, v/v/v) and Leu-enkephalin (m/z 556.2771) was used as the lock mass solution for accurate mass measurements (1 ng/µL in H_2O/CH_3CN/formic acid 50:49.9:0.1, v/v/v). The scan range was

m/z 50-1000 at 0.2 s/scan. The TOF was operated in the resolution mode, providing an average resolving power of 25,000 (FWHM). The acquisition was performed with MassLynx software (V4.2, Waters).

3. Results and discussion

3.1. Impact of LDFP on the electrolyte properties.

The influence of the LDFP additive on the electrolyte properties, i.e. the electrochemical stability window, the viscosity and the ionic conductivity was studied at a concentration of 0.2M (1.92 wt.%) in the base electrolyte (1M $LiPF_6$ in EC/DEC/EMC 1:1:1 v/v), unless otherwise specified. An LDPF concentration of around 3 wt.% could not be exceeded owing to its low solubility in classical Li-ion electrolyte; the $PO_2F_2^-$ anion volume is lower than that of PF_6^- (538.1 and 625.5 $Bohr^3$[27], respectively) and the dissolution energy calculated by density functional theory (DFT) is larger (-5.790 eV for LDFP and -6.254 eV for $LiPF_6$).

Cyclic voltammetry (CV) curves are shown in Fig. 1. From the anodic and cathodic scan, it can be seen that the stability of the electrolyte is not affected by the presence of LDFP in the 0.05-6V domain. No evidence of oxidation of LDFP into the probably highly oxidizing neutral molecule, the peroxodifluorophosphate ($P_2O_4F_4$), is visible. Thus, it can be considered that, based on these CV experiments, LDFP is not electrochemically active in the NMC/graphite cell potential window.

The ionic conductivity of three electrolytes, the base, the base + 0.2M LDFP and an electrolyte containing 0.8M $LiPF_6$ + 0.2M LDFP in the same solvent mixture was measured in the [-10 – +55°C] temperature range, under two different configurations; as a liquid solution (Fig. 2a) and as a liquid impregnated in a porous polypropylene separator (Fig. 2b). Viscosity values obtained at 25°C and 55°C for the two first electrolytes are reported in Fig. 2a.

The conductivity of the base electrolyte (Fig. 2a) was found to decrease by ca. 14% and 17% at 25°C and 55°C, respectively, upon the addition of 0.2M LDFP. Two similar trends have been found in the literature with different carbonate mixtures: Wang et al.[41] found that at 25°C, the original ionic conductivity of 6.34 $mS.cm^{-1}$ decreased by 9.4% with the addition of 2 wt.% of LDFP (base: 1M $LiPF_6$ in EC/DEC 1:3 wt.%). Meanwhile, Zhao et al.[27] found a decrease from 7.31 to 6.72 $mS.cm^{-1}$ (-8%) with the addition of 1 wt.% of LDFP (base: 1M $LiPF_6$ in EC/DMC 1:1 vol.), measured at room temperature.

The decrease in ionic conductivity is in line with the increase of viscosity from 3.8 to 4.4 cP at 25°C and from 2.1 to 2.5 cP at 55°C. At the same time, the formation of LDFP ion pairs can be suspected, instead of complete dissociation as with $LiPF_6$. Among the three electrolytes in the liquid configuration, the 0.8M $LiPF_6$ + 0.2M LDFP electrolyte exhibits the lowest ionic conductivity, especially at high temperatures. Contrarily, Liu et al.[49] reported ionic conductivities of 10 $mS.cm^{-1}$ and 11.6 $mS.cm^{-1}$ (16% more) for the electrolytes 1M $LiPF_6$ and 0.8M $LiPF_6$ - 0.2M LDFP in EC/DEC/EMC 1:1:1 wt.%, respectively. Within the porous polypropylene separator (Fig. 2b), the ionic conductivity of the three electrolytes is divided almost by 10, due to tortuosity[50], and the differences when LDFP is added are very small. As in liquid configuration, the 0.8M $LiPF_6$ + 0.2M LDFP electrolyte presents slightly lower values at temperatures higher than ca. 10°C.

Concerning these differences in ionic conductivity of the electrolytes with and without 0.2M LDFP, they are so small that no real impact on electrochemical performance is expected during cycling of the prototype NMC/Graphite (Gr) pouch cell prototypes.

3.2. Impact of $LiPO_2F_2$ on the electrochemical performance of NMC 622C.

Many studies have compared the cycling performance of relatively low Ni-content NMC-based cells in presence of 0.5 – 3 wt.% of LDFP. At ambient temperature, LDFP addition improved the capacity retention of pouch cells cycled up to different cut-off voltages in the 4.1 - 4.5 V range[24,32,33,43], with NMC111/Gr and NMC532/Gr, within the first 100 cycles. At lower temperatures (0°C and -20°C), better capacity retention has also been reported in NMC532/Gr cells[39]. Nonetheless, upon temperature increase, the capacity retention of NMC532/Gr pouch cell was not or only slightly improved in NMC532/Gr pouch cells at 45°C[45] and 40°C[32] respectively, both with cut-off voltages of 4.2 and 4.3 V. In short, with LDFP electrolyte additive, increased cycling performance of relatively low Ni content NMCs-containing cells can be achieved from -20 to 40°C. However, this additive hardly shows any improvement at a higher temperature around 45°C in full cells.

In the last two years, performances of Ni-rich cathode (NCA and NMC811)-containing cells have been evaluated at room temperature and with 1 wt.% of LDFP in electrolyte during 200 [30,34] and 3000 cycles[52]. Although the composition of the electrolyte and the potential window are different, the capacity retention is, again, higher in presence of LDFP. Besides, experiencing higher cycling temperatures[52] (40 and 55°C) was found to result in quite better cycling performances, immediately from the beginning of cycling.

Considering the above, NMC 622/Gr pouch cell prototypes performances were investigated at 55°C. As shown in Fig. 3, the representative electrochemical capacity curves exhibit enhanced capacity retention with 0.2M LDFP (82.6 versus 79.6% without LDFP at 200 cycles). As generally stated in the literature, the beneficial impact on capacity retention becomes visible already during the first 100 cycles.

To better understand the beneficial impact of this additive, we studied the degradation products of electrolytes by means of infrared and mass spectrometry techniques. Fit-to-purpose experimental procedures were implemented for each of these analyses.

3.3 FT-IR study of SEI and CEI layers.

Electrolyte degradation salts precipitated in SEI and CEI layers formed at the surface of graphite and NMC622 composite powders (active material and C45 in 9:1 mass ratio) were characterized by means of FT-IR after one cycle at 20 and 55°C. Even after greatly enlarging the NMC622 composite spectra, no discernable peaks were revealed in the presence or absence of the additive, which is in sharp contrast to the usual observation in the literature of phosphate species by XPS. The conclusion can be drawn that the cycling conditions or NMC material might not be appropriate for CEI analysis through IR technique; the study of CEI layers composition will be further discussed later in the paper.

Furthermore, as shown in Fig. 4a, irrespective of the temperature, 25 and 55°C, the composition of the SEI is not much influenced by the presence of LDFP electrolyte additive. Indeed, most of the vibration bands are observed in spectra of the SEI formed from the base electrolyte (called base-SEI) and from the LDFP-containing electrolyte (LDFP-SEI). Marked with stars and hash characters in the figure, they are assigned to the reduction products of carbonates solvents, lithium alkyl carbonates and Li_2CO_3[53], respectively. This result is in good agreement with the SEI-related dQ/dV derivative peaks (Fig. 5), from which conclusion can be drawn that LDFP does not prevent solvents reduction processes at the surface of graphite composite powder. The electrochemical reduction of the carbonate solvents (mostly EC) takes place around 0.7-0.9 V *vs*. Li/Li^+ at 25 and 55°C respectively.

However, supplementary bands or more pronounced shoulders appear in the LDFP-SEIs, at both temperatures, in the 900-1300 cm^{-1} range, typical of C-O stretching vibrations but also of the frequency range of phosphate- or fluorophosphate-type compounds with P–O, P–O–C and P–F functional groups[54]. LDFP displays four bands in this region (Fig. 4b)[55] at 885, 930,

1150 and 1270 cm^{-1} corresponding to P–F and O=P–O symmetric and asymmetric stretching vibrations respectively. The observation in the LDFP-SEI spectra of a peak at 930 cm^{-1} of low intensity may suggest that a small amount of LDFP is precipitated in the SEI.

The set of at least two broad peaks between 960 – 1070 cm^{-1} that, according to Becker et al.[56], corresponds to P–O–C stretching vibration, implies that, in presence of 0.2M LDFP in the electrolyte, the SEI contains (or contains more) phosphate species with alkyl groups attached. The underlying mechanism will be detailed below, in light of the results of the analysis of electrolyte degradation products.

3.4. Analysis of decomposition products in the electrolyte.

Electrolyte aging is mainly investigated through the use of GC-MS[57–60] and LC-MS[60–62] which are complementary techniques. The first one allows to identify volatile compounds (low mass range). LC-MS proved its capacity in identifying less volatile compounds such as ethylene oxide oligomers and phosphates, enabling us, in this study, to establish electrochemically/chemically driven degradation mechanisms.

Analysis of the composition of the LDFP-SEI entails the presence of more organo-(fluoro)phosphorus compounds, the formation mechanism of which could have altered the nature of the degradation products accumulated in the electrolyte. In the literature, only Qian et al.[42] have focused on the composition of the electrolyte very recently. They analyzed, through gas and liquid chromatography/mass spectrometry, the electrolyte composed of 1M $LiPF_6$ and 1 wt.% of LDFP in EC/DEC (3:7 wt.), recovered from NMC 532/Gr cells after 4 cycles at room temperature in the 3 - 4.2 V range. They showed the disappearance of degradation products such as diethyl 2,5-dioxahexane dicarboxylate (DEDOHC). To further clarify the reaction mechanisms, we undertook an in-depth analysis of the electrolyte degradation products. For comparison and data reliability purposes, the same experimental protocol described in our previous paper[62] was followed; the electrolyte was extracted from NMC622/Gr pouch cell prototypes after 34 cycles at 55°C with base and base + 0.2M LDFP electrolytes, and the post-cycling electrolyte was analyzed by UPLC-ESI-HRMS in the positive ion mode.

Figure 6 shows the detected ions according to their m/z value, proposed structure, peak intensity. They have been grouped into two families; carbonate and phosphate. Surprisingly, the base electrolyte contains both families, whereas the base + 0.2M LDFP electrolyte contains mostly phosphate compounds and even in a slightly lower amount.

The carbonate compounds are low-mass oligomers ($n \leq 2$) with ethylene oxide and ethylene carbonate units. The ethylene oxide-based compounds are part of the families called $1'_n$ and $1''_n$ in our previous article[63]. They correspond to ethyl methyl (or diethyl) 2,5-dioxahexane dicarboxylate (EMDOHC, m/z 215.05, called $1'_1$ and DEDOHC, m/z 229.07, called $1''_1$) and their respective ethylene oxide-elongated form (m/z 259.08, called $1'_2$ and m/z 273.09, called $1''_2$), the formation mechanism of which can be electrochemically initiated through Eqs 1, 2 and 3. Note that, at 55°C, the thermally-driven formation of $1'_1$ and $1''_1$ through a PF_5-assisted transesterification process involving the electrolyte solvents, EC and DEC or EMC, could also be considered. As for the ethylene carbonate-based oligomers at m/z 303.07, 317.08, 319,04, 333.06, 405.10, they are produced through a PF_5-assisted transesterification reaction involving EC and the compound $1'_1$ or $1''_1$. Hence, their formation can also be electrochemically or thermally initiated.

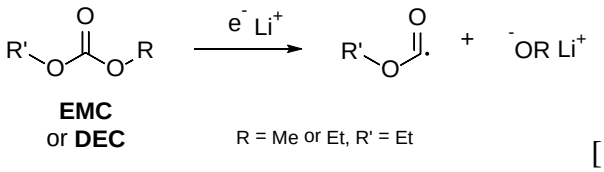

[1]

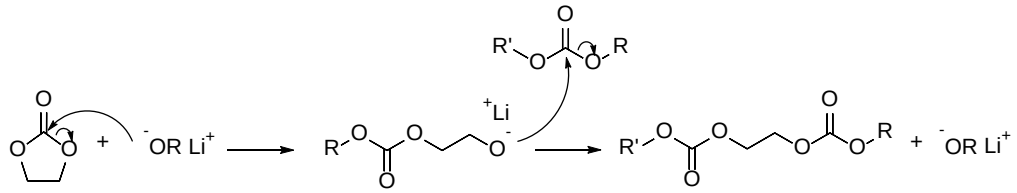

[2]

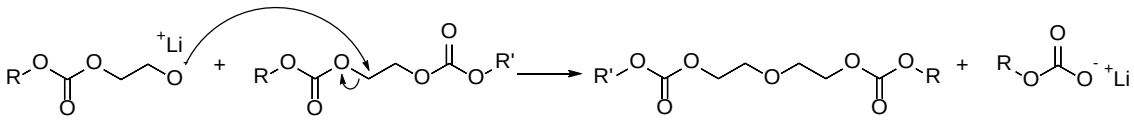

[3]

As displayed in Fig. 6, all of these carbonate compounds are almost non-existent in the case of LDFP electrolyte. As all the cells were cycled at the same temperature of 55°C, it is safe to assume that thermally-initiated transesterification reactions are not prevailing. The formation of the compounds $1'_1$, $1''_1$ and their respective elongated chains is thus essentially electrochemically-initiated. Given this assumption, it is suggested that the alkoxides (RO^-) produced via the electrochemical reduction of EMC or DEC (Eq. 1) can rapidly be trapped by LDFP. As a result, they are no more available for subsequent nucleophilic attack reactions on carbonates to form all the compounds (Eq. 4, reaction 3). Alkoxides are supposed to substitute

fluorine of LDFP (Eq. 4, reaction 1) and yield lithium organo-(fluoro)phosphate salts. The chemical simulation of such substitution reaction has been evidenced through ^{31}P liquid NMR analysis of an EC/DMC (1/1 wt.%) solution containing an equimolar ratio of MeOLi and LDFP, after storage at 55°C for 1 week. Three doublets were observed and their chemical shifts reported in Table 1 can respectively be attributed to $OPOF_2^-$, $OPOF(OCH_3)^-$ and $OPOF(OC_2H_4OCO_2CH_3)^-$ anions.

molecules	$\delta(^{31}P)$ / ppm	J_{P-F} / Hz	J_{P-H} / Hz
	-17	928	
	-5	902	11
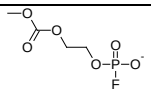	-7	904	7

Table 1. ^{31}P NMR analysis data from chemical reactivity between MeOLi and LDFP experiment

This observation indicates that alkoxide (Eq. 4, reaction 1) but also Intermediary A (Eq. 4, reaction 2) anions can substitute one fluorine anion of LDFP to yield organo-fluorophosphate salts. This result underpins hereabove FT-IR results. Indeed, the produced salts may explain the more pronounced bands in the 900-1300 cm^{-1} range, that were assigned to P-O, P-F and P-O-C vibrations. Hence, a higher amount of lithium organo-fluorophosphate would be part of the SEI in presence of LDFP in electrolyte.

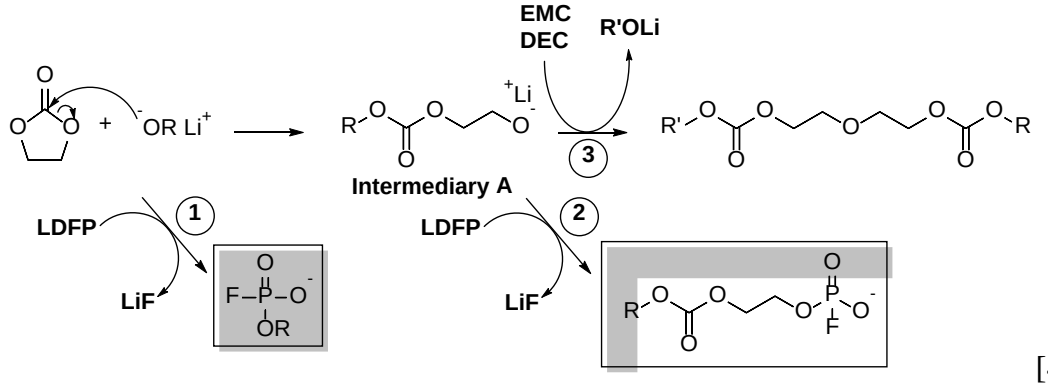

[4]

On the contrary, phosphate compounds are still present with the LDFP electrolyte, although in lower quantities. The phosphate group is produced from the degradation of $LiPF_6$ into PF_5 and LiF, followed by the reaction with residual water to yield HF and POF_3[64–66]. As explained in our previous article[62], the organo-fluorophosphates are the result of subsequent nucleophilic substitution reactions of fluorine by electrochemically-produced anions (alkoxides, intermediary A and lengthened chains) (Eq.5). Their presence thus indicates that anions can concomitantly be scavenged by both types of phosphates; LDFP and water-derived POF_3, leaving, along with LiF, charged and neutral molecules, respectively. The quasi absence

of carbonate compounds in LDFP electrolyte indicates that these anions are more prone to fluorine substitution reactions than nucleophilic attack reactions on carbonates.

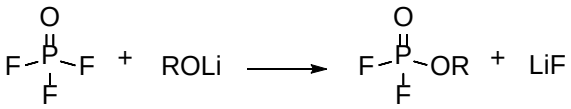

[5]

To sum up, in base electrolyte, alkoxides anions RO^- originating from the reduction of linear solvents bring about the formation of ethylene oxide and ethylene carbonates oligomers as well as phosphate-ending oligomers due to reaction of $LiPF_6$ (PF_5) with water. Adding LDFP in electrolyte shows that the reaction of alkoxides and Intermediary A with LDFP is kinetically favored (Eq. 4, reaction 1 and 2), thus preventing the formation of the above-reported ethylene oxide and ethylene carbonate oligomers (Eq. 4, reaction 3).

It is worth noting that methoxide anions, MeO^-, resulting from the linear reduction of DMC could have been quantified after the formation of an SEI[67]. A selective bicyclic boron ester Lewis acid was used as an additive to EC/DMC (1/1 p/w) - $LiPF_6$ salt (1M) electrolyte to trap MeO^-, forming a complex in the electrolyte. Similar to LDFP, the presence of this additive was found not to influence the SEI-forming electrochemical reduction processes; the capacity consumed between 0.9-0.6 V vs $Li°/Li^+$ remaining unchanged. It had been indirectly demonstrated that a non-negligible percentage of this capacity, around 16%, was dedicated to reducing DMC (the remaining part, 84%, for EC reduction) and forming MeO^-. Interestingly, like LDFP, the boron ester molecule enables the trapping of anions, thus preventing the formation of carbonate oligomers, but without releasing F- and P-based SEI.

3.5. Discussion on interphases LDFP impact

3.5.1 SEI

As a result of the fluorine substitution reactions, the amount of LiF in the interphase layers is expected to increase, which was usually observed through XPS analysis (F1s: 685-686.5 eV) with LDFP electrolyte[26,34,44,45]. Furthermore, both FT-IR and XPS techniques agree to indicate the presence of additional P, O, F-based components in SEI; FT-IR spectra exhibit more intense bands in the 900-1300 cm^{-1} while most of the P2p XPS spectra reported in the literature have shown more intense bands in the 134-137eV range. However, their identification remains challenging. In XPS studies, these bands are mainly assumed to be precipitated inorganic salts; $Li_xPF_yO_z$ (134-136 eV), Li_xPF_y (136-137 eV) and LDFP (~133.5 eV). LDFP can be simply precipitated when present as an additive in electrolyte, due to its low solubility.

Noteworthy, LDFP can also result from the reaction between the Li_2CO_3[47,68] reduction compound and $LiPF_6$ following Eq. 6.

$$2Li_2CO_3 + LiPF_6 \rightarrow LiPO_2F_2 + 2CO_2 + 4LiF \quad [6]$$

The electrolyte ESI-HRMS analysis led us to conclude that the additional P, O, F-based compounds could also correspond to organo-(fluoro)phosphate salts. It is worth noting that they are not produced from direct electrochemical reduction processes but from substitution reactions in solution. Therefore, they are not expected to be located near the graphite/SEI interface but rather in the outermost part of the SEI. In fact, at the graphite lithiation stage, the concentration of lithium ions and anions produced by reduction increases at the interface, decreasing the solubility of lithium salts and thus enabling the precipitation of these LDFP-derived salts. When the system shifts to the delithiation stage, the interface is no longer a zone with a high concentration of salts, which can lead to their solubilisation. It is presumed that this process is hampered by the coexistence of insoluble LiF, leaving some of the organo-(fluoro)phosphate salts trapped in the SEI. The resulting overcovering layer would enhance the SEI passivation properties upon cycling, even at 55°C.

Interestingly, in commercial Li-ion cells, the carboxymethyl cellulose (CMC) binder is also known to act as a perfectly covering passivation layer and thus, participates in the negative electrode cycling performance improvement. In addition to the effect described above, it could be assumed that LDFP reacts with CMC by a nucleophilic substitution reaction according to Eq. 7, and thus endow CMC-based SEI with even more improved passivation properties due to a steric effect and the presence of insoluble LiF. The probable occurrence of such a bond between the binder and this additive should be demonstrated, in the same way as studies revealing a covalent bond by the esterification reaction between CMC carboxylate and the hydroxyl groups present at the surface of a silicon anode, under low pH conditions[69].

$$CMC–COONa + LiPO_2F_2 \rightarrow CMC–COOPO_2FNa + LiF \quad [7]$$

3.5.2 CEI

At the positive electrode, after one cycle, our FT-IR spectra showed no band relative to a CEI layer, even with LDFP electrolyte. However, in the literature, TEM images [24,28,29,70] of positive active particles surfaces after different numbers of cycles (up to 300 cycles) reveal a thin CEI layer of about 8 to 20 nm in LDFP electrolyte compared to 0 to 150 nm in the base electrolyte.

In the literature, a greater amount of P, F, O-based species is observed in the CEI by XPS with LDFP electrolyte but their origin is not clearly explained. Recently, Klein et al.[36] proposed the formation of PO_4^{3-} and PO_3F^{2-}species, leaving precipitated Li_3PO_4 and Li_2PO_3F salts in both interphase layers. However, their formation seems difficult to envisage because it would require the presence of water and the LDFP hydrolysis reaction would rather produce the mono-fluoro phosphoric and phosphoric acids, $HFPO_3^-$ and $H_2PO_4^-$ (Eqs 8 and 9) whose hydrogens would be difficult to ionize to yield PO_4^{3-} and PO_3F^{2-} owing to the relatively low donor number of the electrolyte carbonate solvents mixture (DN ~15).

$$LiPO_2F_2 + H_2O \rightarrow LiPO_2F(OH) + HF \quad [8]$$

$$LiPO_2F_2 + 2H_2O \rightarrow LiPO_2(OH)_2 + 2HF \quad [9]$$

On the other hand, the authors proved, through EDX analysis on graphite electrode, the near absence of TMs coming possibly from HF-driven positive electrode dissolution processes, when LDFP is added in the electrolyte. It is worth mentioning that dissolved TMs migrate to the negative electrode surface to be reduced. As proved with manganese[71], the newly formed metal can decrease the interface impedance but then acts as nucleation sites for further electrolyte degradation and SEI growth. The same authors explain the prevention of such TMs deposition via their complexation with these hypothetical PO_4^{3-} and PO_3F^{2-} species, without giving the formula of the metallic complex. One could have imagined the formation of $Ni_3(PO_4)_2$ and $NiPO_3F$ that would be precipitated in CEI. Actually, it has been reported that a 20 nm thick $Ni_3(PO_4)_2$ coating on NMC[72] and NCA[73] enhances the high rate performances, especially at high cut-off voltage.

In the literature, reference is also made to the existence of $Ni(PO_2F_2)_2$[54] and $Ni(PO_2F_2)_2.HPO_2F_2$[74] salts. The formation of these compounds in the CEI layer would therefore be conceivable in the presence of LDFP and also water for the second compound; HPO_2F_2 resulting from POF_3 hydrolysis following Eq. 10. They would form a passivating CEI layer that would prevent HF attack related TMs dissolution and further associated electrode cross-talk reactions[19]. The surface reactions are exemplified in Eqs 11 and 12.

$$OPF_3 + H_2O \rightarrow OPF_2(OH) + HF \quad [10]$$

$$LiNi_{0.6}Mn_{0.2}Co_{0.2}O_2 + 2\varepsilon LiPO_2F_2 \rightarrow \varepsilon Ni(PO_2F_2)_2 + \varepsilon Li_2O + LiNi_{0.6-\varepsilon}Mn_{0.2}Co_{0.2}O_{2-\varepsilon} \quad [11]$$

$$LiNi_{0.6}Mn_{0.2}Co_{0.2}O_2 + 2\varepsilon OPF_2(OH) \rightarrow \varepsilon Ni(PO_2F_2)_2 + \varepsilon H_2O + LiNi_{0.6-\varepsilon}Mn_{0.2}Co_{0.2}O_{2-\varepsilon} \quad [12]$$

Note that Li_2O as surface species resulting from synthesis or as produced from Eq. 12, can then react with $LiPF_6$ to yield LDFP.

Considering the above results and the literature[75], one can also envisage the formation of Ni organophosphate salts $Ni(OOP(OR)_2)_2$ (with R=Me or Et)precipitated in the CEI, which would have the same beneficial effect on the TMs dissolution as the Ni fluorophosphates, $Ni(PO_2F_2)_2$ and $Ni(PO_2F_2)_2.HPO_2F_2$. Hence, Ni fluoro or organophosphates salts could be considered to be formed in the thin CEI layer.

4. Conclusion

With the help of an extensive bibliographic analysis, this work provides new insight into the reactivity of LDFP electrolyte additive (Fig. 7). Evidence is given that this additive is not electrochemically active in the 0-4.3 V functioning potential window of NMC/graphite-based cells, and therefore does not behave as a typical additive that reduces or oxidizes to generate reinforced SEI or CEI layers. LDFP does not prevent electrolyte carbonate solvents from being reduced during the first charge, so that the classical lithium carbonate and alkyl carbonate salts are formed in the SEI. However, as a result of these solvents electrochemical reduction, its fluorine is subjected to nucleophilic substitution by RO^- and its derivatives, leaving additional LiF and lithium organo-fluorophosphate precipitated in SEI. On the other hand, the CEI composition has been discussed and it is concluded that it may be composed of Ni fluoro or organophosphate components. These F, P-based compounds and LiF are believed to confer SEI and CEI better passivation properties, hindering, for instance, thermally favored SEI dissolution and TMs dissolution driven crosstalk reactions and thus allowing improved capacity retention of Li-ion pouch cells achievement.

Acknowledgments: The financial support from the Association Nationale de la Recherche et de la Technologie (ANRT, France) is gratefully acknowledged. The authors thank Guangzhou Tinci Materials Technology Co., Ltd for $LiPO_2F_2$ supply and Umicore for NMC cathode materials supply.

References

[1] M. Fichtner, Recent Research and Progress in Batteries for Electric Vehicles, Batteries & Supercaps. 5 (2022) e202100224. https://doi.org/10.1002/batt.202100224.

[2] T.Y. Chian, W.L.J. Wei, E.L.M. Ze, L.Z. Ren, Y.E. Ping, N.Z.A. Bakar, M. Faizal, S. Sivakumar, A Review on Recent Progress of Batteries for Electric Vehicles, 14 (2019) 21.

[3] M. Marinaro, D. Bresser, E. Beyer, P. Faguy, K. Hosoi, H. Li, J. Sakovica, K. Amine, M. Wohlfahrt-Mehrens, S. Passerini, Bringing forward the development of battery cells for automotive applications: Perspective of R&D activities in China, Japan, the EU and the USA, Journal of Power Sources. 459 (2020) 228073. https://doi.org/10.1016/j.jpowsour.2020.228073.

[4] H. Zhang, C. Li, G.G. Eshetu, S. Laruelle, S. Grugeon, K. Zaghib, C. Julien, A. Mauger, D. Guyomard, T. Rojo, N. Gisbert-Trejo, S. Passerini, X. Huang, Z. Zhou, P. Johansson, M. Forsyth, From Solid-Solution Electrodes and the Rocking-Chair Concept to Today's Batteries, Angew. Chem. Int. Ed. 59 (2020) 534–538. https://doi.org/10.1002/anie.201913923.

[5] E. Peled, The Electrochemical Behavior of Alkali and Alkaline Earth Metals in Nonaqueous Battery Systems—The Solid Electrolyte Interphase Model, J. Electrochem. Soc. 126 (1979) 2047–2051. https://doi.org/10.1149/1.2128859.

[6] S. Grugeon, P. Jankowski, D. Cailleu, C. Forestier, L. Sannier, M. Armand, P. Johansson, S. Laruelle, Towards a better understanding of vinylene carbonate derived SEI-layers by synthesis of reduction compounds, Journal of Power Sources. 427 (2019) 77–84. https://doi.org/10.1016/j.jpowsour.2019.04.061.

[7] C. Forestier, S. Grugeon, C. Davoisne, A. Lecocq, G. Marlair, M. Armand, L. Sannier, S. Laruelle, Graphite electrode thermal behavior and solid electrolyte interphase investigations: Role of state-of-the-art binders, carbonate additives and lithium bis(fluorosulfonyl)imide salt, Journal of Power Sources. 330 (2016) 186–194. https://doi.org/10.1016/j.jpowsour.2016.09.005.

[8] M. Xu, W. Li, B.L. Lucht, Effect of propane sultone on elevated temperature performance of anode and cathode materials in lithium-ion batteries, Journal of Power Sources. 193 (2009) 804–809. https://doi.org/10.1016/j.jpowsour.2009.03.067.

[9] K. Lee, H. Jung, J. Chung, K.S. Kim, J. Song, J. Park, Unraveling the effect of succinonitrile additive on cycling performance in cylindrical lithium-ion battery, Electrochimica Acta. 281 (2018) 274–281. https://doi.org/10.1016/j.electacta.2018.05.175.

[10] R. Jung, M. Metzger, F. Maglia, C. Stinner, H.A. Gasteiger, Oxygen Release and Its Effect on the Cycling Stability of LiNixMnyCozO2 (NMC) Cathode Materials for Li-Ion Batteries, J. Electrochem. Soc. 164 (2017) A1361. https://doi.org/10.1149/2.0021707jes.

[11] P. Teichert, G.G. Eshetu, H. Jahnke, E. Figgemeier, Degradation and Aging Routes of Ni-Rich Cathode Based Li-Ion Batteries, Batteries. 6 (2020) 8. https://doi.org/10.3390/batteries6010008.

[12] J.L. Tebbe, A.M. Holder, C.B. Musgrave, Mechanisms of LiCoO2 Cathode Degradation by Reaction with HF and Protection by Thin Oxide Coatings, ACS Appl. Mater. Interfaces. 7 (2015) 24265–24278. https://doi.org/10.1021/acsami.5b07887.

[13] S.F. Lux, I.T. Lucas, E. Pollak, S. Passerini, M. Winter, R. Kostecki, The mechanism of HF formation in LiPF6 based organic carbonate electrolytes, Electrochemistry Communications. 14 (2012) 47–50. https://doi.org/10.1016/j.elecom.2011.10.026.

[14] W. Li, Review—An Unpredictable Hazard in Lithium-ion Batteries from Transition Metal Ions: Dissolution from Cathodes, Deposition on Anodes and Elimination Strategies, J. Electrochem. Soc. 167 (2020) 090514. https://doi.org/10.1149/1945-7111/ab847f.

[15] D.R. Gallus, R. Schmitz, R. Wagner, B. Hoffmann, S. Nowak, I. Cekic-Laskovic, R.W. Schmitz, M. Winter, The influence of different conducting salts on the metal dissolution and capacity fading of NCM cathode material, Electrochimica Acta. 134 (2014) 393–398. https://doi.org/10.1016/j.electacta.2014.04.091.
[16] R. Sahore, D.C. O'Hanlon, A. Tornheim, C.-W. Lee, J.C. Garcia, H. Iddir, M. Balasubramanian, I. Bloom, Revisiting the Mechanism Behind Transition-Metal Dissolution from Delithiated $LiNi_x Mn_y Co_z O_2$ (NMC) Cathodes, J. Electrochem. Soc. 167 (2020) 020513. https://doi.org/10.1149/1945-7111/ab6826.
[17] H. Zheng, Q. Sun, G. Liu, X. Song, V.S. Battaglia, Correlation between dissolution behavior and electrochemical cycling performance for LiNi1/3Co1/3Mn1/3O2-based cells, Journal of Power Sources. 207 (2012) 134–140. https://doi.org/10.1016/j.jpowsour.2012.01.122.
[18] J. Wandt, A. Freiberg, R. Thomas, Y. Gorlin, A. Siebel, R. Jung, H.A. Gasteiger, M. Tromp, Transition metal dissolution and deposition in Li-ion batteries investigated by operando X-ray absorption spectroscopy, J. Mater. Chem. A. 4 (2016) 18300–18305. https://doi.org/10.1039/C6TA08865A.
[19] R. Jung, F. Linsenmann, R. Thomas, J. Wandt, S. Solchenbach, F. Maglia, C. Stinner, M. Tromp, H.A. Gasteiger, Nickel, Manganese, and Cobalt Dissolution from Ni-Rich NMC and Their Effects on NMC622-Graphite Cells, J. Electrochem. Soc. 166 (2019) A378–A389. https://doi.org/10.1149/2.1151902jes.
[20] S. Zhang, J. Ma, Z. Hu, G. Cui, L. Chen, Identifying and Addressing Critical Challenges of High-Voltage Layered Ternary Oxide Cathode Materials, Chem. Mater. 31 (2019) 6033–6065. https://doi.org/10.1021/acs.chemmater.9b01557.
[21] A.M. Haregewoin, A.S. Wotango, B.-J. Hwang, Electrolyte additives for lithium ion battery electrodes: progress and perspectives, Energy Environ. Sci. 9 (2016) 1955–1988. https://doi.org/10.1039/C6EE00123H.
[22] Z. Zhang, X. Wang, Y. Bai, C. Wu, Charactering and optimizing cathode electrolytes interface for advanced rechargeable batteries: Promises and challenges, Green Energy & Environment. (2021) S2468025721001138. https://doi.org/10.1016/j.gee.2021.05.012.
[23] A. Schulz, P. Garcia-Juan, Fabrication de lipo2f2 à partir de pof3 ou de pf5, 2012. https://patents.google.com/patent/WO2012016924A1/fr (accessed December 19, 2018).
[24] J. Chen, L. Xing, X. Yang, X. Liu, T. Li, W. Li, Outstanding electrochemical performance of high-voltage LiNi1/3Co1/3Mn1/3O2 cathode achieved by application of LiPO2F2 electrolyte additive, Electrochimica Acta. 290 (2018) 568–576. https://doi.org/10.1016/j.electacta.2018.09.077.
[25] Q.Q. Liu, L. Ma, C.Y. Du, J.R. Dahn, Effects of the LiPO2F2 additive on unwanted lithium plating in lithium-ion cells, Electrochimica Acta. 263 (2018) 237–248. https://doi.org/10.1016/j.electacta.2018.01.058.
[26] Y. Chen, W. Zhao, Q. Zhang, G. Yang, J. Zheng, W. Tang, Q. Xu, C. Lai, J. Yang, C. Peng, Armoring LiNi1/3Co1/3Mn1/3O2 Cathode with Reliable Fluorinated Organic–Inorganic Hybrid Interphase Layer toward Durable High Rate Battery, Advanced Functional Materials. 30 (2020) 2000396. https://doi.org/10.1002/adfm.202000396.
[27] D. Zhao, S. Song, X. Ye, P. Wang, J. Wang, Y. Wei, C. Li, L. Mao, H. Zhang, S. Li, New insight into the mechanism of LiPO2F2 on the interface of high-voltage cathode LiNi0.5Mn1.5O4 with truncated octahedral structure, Applied Surface Science. 491 (2019) 595–606. https://doi.org/10.1016/j.apsusc.2019.06.146.
[28] B. Liu, H. Zhou, C. Yin, H. Guan, J. Li, Enhanced electrochemical performance of LiNi0.5Mn1.5O4 cathode by application of LiPF2O2 for lithium difluoro(oxalate)borate electrolyte, Electrochimica Acta. 321 (2019) 134690. https://doi.org/10.1016/j.electacta.2019.134690.

[29] Z. Yu, M. Bai, W. Song, S. Hong, B. Hong, Y. Lai, Y. Liu, Influence of lithium difluorophosphate additive on the high voltage LiNi0.8Co0.1Mn0.1O2/graphite battery, Ceramics International. 47 (2021) 157–162. https://doi.org/10.1016/j.ceramint.2020.08.119.
[30] J. Wang, D. Zhao, Y. Cong, N. Zhang, P. Wang, X. Fu, X. Cui, Analyzing the Mechanism of Functional Groups in Phosphate Additives on the Interface of $LiNi_{0.8}Co_{0.15}Al_{0.05}O_2$ Cathode Materials, ACS Appl. Mater. Interfaces. 13 (2021) 16939–16951. https://doi.org/10.1021/acsami.0c21535.
[31] K.-E. Kim, J.Y. Jang, I. Park, M.-H. Woo, M.-H. Jeong, W.C. Shin, M. Ue, N.-S. Choi, A combination of lithium difluorophosphate and vinylene carbonate as reducible additives to improve cycling performance of graphite electrodes at high rates, Electrochemistry Communications. 61 (2015) 121–124. https://doi.org/10.1016/j.elecom.2015.10.013.
[32] L. Ma, L. Ellis, S.L. Glazier, X. Ma, Q. Liu, J. Li, J.R. Dahn, LiPO2F2 as an Electrolyte Additive in Li[Ni0.5Mn0.3Co0.2]O2/Graphite Pouch Cells, J. Electrochem. Soc. 165 (2018) A891–A899. https://doi.org/10.1149/2.0381805jes.
[33] Q. Lei, T. Yang, X. Zhao, W. Fan, W. Wang, L. Yu, S. Guo, X. Zuo, R. Zeng, J. Nan, Lithium difluorophosphate as a multi-functional electrolyte additive for 4.4 V LiNi0.5Co0.2Mn0.3O2/graphite lithium ion batteries, Journal of Electroanalytical Chemistry. 846 (2019) 113141. https://doi.org/10.1016/j.jelechem.2019.05.023.
[34] Y. Li, B. Cheng, F. Jiao, K. Wu, The Roles and Working Mechanism of Salt-Type Additives on the Performance of High-Voltage Lithium-Ion Batteries, ACS Appl. Mater. Interfaces. 12 (2020) 16298–16307. https://doi.org/10.1021/acsami.9b22360.
[35] C. Wang, M. Liu, D. Huang, Q. Wang, A. Mei, W. Fan, J. Ye, W. Yang, High-voltage LiNi0.4Co0.4Mn0.2O2/graphite pouch battery cycled at 4.5 V with a LiDFP-based electrolyte, Ionics. 27 (2021) 4135–4142. https://doi.org/10.1007/s11581-021-04193-9.
[36] S. Klein, P. Harte, S. van Wickeren, K. Borzutzki, S. Röser, P. Bärmann, S. Nowak, M. Winter, T. Placke, J. Kasnatscheew, Re-evaluating common electrolyte additives for high-voltage lithium ion batteries, Cell Reports Physical Science. 2 (2021) 100521. https://doi.org/10.1016/j.xcrp.2021.100521.
[37] School of Metallurgy and Environment, Central South University, Changsha Hunan 410083, China, W. Song, LiPO2F2 as a LiPF6 Stablizer Additive to Improve the high-temperature Performance of the NCM811/SiOx@C Battery, Int. J. Electrochem. Sci. (2019) 9069–9079. https://doi.org/10.20964/2019.09.55.
[38] J.-W. Seok, J. Lee, T. Rodgers, D.-H. Ko, J.-H. Shim, Effect of LiPO2F2 Electrolyte Additive on Surface Electrical Properties of LiNi0.6Co0.2Mn0.2O2 Cathode, Trans. Electr. Electron. Mater. 20 (2019) 548–553. https://doi.org/10.1007/s42341-019-00151-5.
[39] B. Yang, H. Zhang, L. Yu, W. Fan, D. Huang, Lithium difluorophosphate as an additive to improve the low temperature performance of LiNi0.5Co0.2Mn0.3O2/graphite cells, Electrochimica Acta. 221 (2016) 107–114. https://doi.org/10.1016/j.electacta.2016.10.037.
[40] C. Wang, L. Yu, W. Fan, R. Liu, J. Liu, L. Ouyang, L. Yang, M. Zhu, Enhanced high-voltage cyclability of LiNi0.5Co0.2Mn0.3O2-based pouch cells via lithium difluorophosphate introducing as electrolyte additive, Journal of Alloys and Compounds. 755 (2018) 1–9. https://doi.org/10.1016/j.jallcom.2018.05.005.
[41] C. Wang, L. Yu, W. Fan, J. Liu, L. Ouyang, L. Yang, M. Zhu, Lithium Difluorophosphate As a Promising Electrolyte Lithium Additive for High-Voltage Lithium-Ion Batteries, ACS Appl. Energy Mater. 1 (2018) 2647–2656. https://doi.org/10.1021/acsaem.8b00342.

[42] Y. Qian, S. Hu, X. Zou, Z. Deng, Y. Xu, Z. Cao, Y. Kang, Y. Deng, Q. Shi, K. Xu, Y. Deng, How electrolyte additives work in Li-ion batteries, Energy Storage Materials. 20 (2019) 208–215. https://doi.org/10.1016/j.ensm.2018.11.015.
[43] G. Yang, J. Shi, C. Shen, S. Wang, L. Xia, H. Hu, H. Luo, Y. Xia, Z. Liu, Improving the cyclability performance of lithium-ion batteries by introducing lithium difluorophosphate ($LiPO_2F_2$) additive, RSC Advances. 7 (2017) 26052–26059. https://doi.org/10.1039/C7RA03926C.
[44] A.S. Keefe, R. Weber, I.G. Hill, J.R. Dahn, Studies of the SEI layers in $Li(Ni_{0.5}Mn_{0.3}Co_{0.2})O_2$ /Artificial Graphite Cells after Formation and after Cycling, J. Electrochem. Soc. 167 (2020) 120507. https://doi.org/10.1149/1945-7111/abaa1b.
[45] Y. Qian, S. Hu, X. Zou, Z. Deng, Y. Xu, Z. Cao, Y. Kang, Y. Deng, Q. Shi, K. Xu, Y. Deng, How electrolyte additives work in Li-ion batteries, Energy Storage Materials. 20 (2019) 208–215. https://doi.org/10.1016/j.ensm.2018.11.015.
[46] H. Chen, B. Liu, Y. Wang, H. Guan, H. Zhou, Insight into wide temperature electrolyte based on lithiumdifluoro(oxalate)borate for high voltage lithium-ion batteries, Journal of Alloys and Compounds. 876 (2021) 159966. https://doi.org/10.1016/j.jallcom.2021.159966.
[47] A.C. Martinez, S. Grugeon, D. Cailleu, M. Courty, P. Tran-Van, B. Delobel, S. Laruelle, High reactivity of the nickel-rich LiNi1-x-yMnxCoyO2 layered materials surface towards H2O/CO2 atmosphere and LiPF6-based electrolyte, Journal of Power Sources. 468 (2020) 228204. https://doi.org/10.1016/j.jpowsour.2020.228204.
[48] D.S. Hall, R. Gauthier, A. Eldesoky, V.S. Murray, J.R. Dahn, New Chemical Insights into the Beneficial Role of Al2O3 Cathode Coatings in Lithium-ion Cells, ACS Appl. Mater. Interfaces. (2019). https://doi.org/10.1021/acsami.8b22743.
[49] L. Liu, S. Gu, S. Wang, X. Zhang, S. Chen, A $LiPO_2F_2$ /LiPF 6 dual-salt electrolyte enabled stable cycling performance of nickel-rich lithium ion batteries, RSC Advances. 10 (2020) 1704–1710. https://doi.org/10.1039/C9RA09841K.
[50] J. Landesfeind, J. Hattendorff, A. Ehrl, W.A. Wall, H.A. Gasteiger, Tortuosity Determination of Battery Electrodes and Separators by Impedance Spectroscopy, J. Electrochem. Soc. 163 (2016) A1373. https://doi.org/10.1149/2.1141607jes.
[51] Q. Lei, T. Yang, X. Zhao, W. Fan, W. Wang, L. Yu, S. Guo, X. Zuo, R. Zeng, J. Nan, Lithium difluorophosphate as a multi-functional electrolyte additive for 4.4V LiNi0.5Co0.2Mn0.3O2/graphite lithium ion batteries, Journal of Electroanalytical Chemistry. 846 (2019) 113141. https://doi.org/10.1016/j.jelechem.2019.05.023.
[52] W. Song, J. Harlow, E. Logan, H. Hebecker, M. Coon, L. Molino, M. Johnson, J. Dahn, M. Metzger, A Systematic Study of Electrolyte Additives in Single Crystal and Bimodal $LiNi_{0.8}Mn_{0.1}Co_{0.1}O_2$ /Graphite Pouch Cells, J. Electrochem. Soc. 168 (2021) 090503. https://doi.org/10.1149/1945-7111/ac1e55.
[53] L. Gireaud, S. Grugeon, S. Laruelle, S. Pilard, J.-M. Tarascon, Identification of Li Battery Electrolyte Degradation Products Through Direct Synthesis and Characterization of Alkyl Carbonate Salts, Journal of The Electrochemical Society. 152 (2005) A850. https://doi.org/10.1149/1.1872673.
[54] T.H. Tan, preparation and properties of metal difluorophosphates, University of British Columbia, 1970.
[55] G. Han, Y. Wang, H. Li, Z. Yang, S. Pan, The first lithium difluorophosphate $LiPO_2F_2$ with a neutral polytetrahedral microporous architecture, Chemical Communications. 55 (2019) 1817–1820. https://doi.org/10.1039/C8CC10158B.
[56] G. Becker, L.-M. Ackermann, E. Schechtel, M. Klapper, W. Tremel, F.R. Wurm, Joining Two Natural Motifs: Catechol-Containing Poly(phosphoester)s, Biomacromolecules. 18 (2017) 767–777. https://doi.org/10.1021/acs.biomac.6b01613.

[57] M. Arakawa, J. Yamaki, Anodic oxidation of propylene carbonate and ethylene carbonate on graphite electrodes, Journal of Power Sources. 54 (1995) 250–254. https://doi.org/10.1016/0378-7753(94)02078-H.
[58] B.A. Johnson, R.E. White, Characterization of commercially available lithium-ion batteries, (n.d.) 7.
[59] G. Gachot, P. Ribière, D. Mathiron, S. Grugeon, M. Armand, J.-B. Leriche, S. Pilard, S. Laruelle, Gas Chromatography/Mass Spectrometry As a Suitable Tool for the Li-Ion Battery Electrolyte Degradation Mechanisms Study, Anal. Chem. 83 (2011) 478–485. https://doi.org/10.1021/ac101948u.
[60] V. Kraft, W. Weber, B. Streipert, R. Wagner, C. Schultz, M. Winter, S. Nowak, Qualitative and quantitative investigation of organophosphates in an electrochemically and thermally treated lithium hexafluorophosphate-based lithium ion battery electrolyte by a developed liquid chromatography-tandem quadrupole mass spectrometry method, RSC Adv. 6 (2016) 8–17. https://doi.org/10.1039/C5RA23624J.
[61] S. Takeda, W. Morimura, Y.-H. Liu, T. Sakai, Y. Saito, Identification and formation mechanism of individual degradation products in lithium-ion batteries studied by liquid chromatography/electrospray ionization mass spectrometry and atmospheric solid analysis probe mass spectrometry: Identification of degradation products in LIBs by LC/ESI-MS and ASAP-MS, Rapid Commun. Mass Spectrom. 30 (2016) 1754–1762. https://doi.org/10.1002/rcm.7652.
[62] S. Rigaud, A.C. Martinez, T. Lombard, S. Grugeon, P. Tran-Van, S. Pilard, S. Laruelle, Mass Spectrometry Analysis of NMC622/Graphite Li-Ion Cells Electrolyte Degradation Products after Storage and Cycling, J. Electrochem. Soc. 169 (2022) 010502. https://doi.org/10.1149/1945-7111/ac44bb.
[63] G. Gachot, S. Grugeon, M. Armand, S. Pilard, P. Guenot, J.-M. Tarascon, S. Laruelle, Deciphering the multi-step degradation mechanisms of carbonate-based electrolyte in Li batteries, Journal of Power Sources. 178 (2008) 409–421. https://doi.org/10.1016/j.jpowsour.2007.11.110.
[64] Z. Song, L. Zheng, P. Cheng, X. Wang, H. Wu, Q. Ma, J. Liu, W. Feng, J. Nie, H. Yu, X. Huang, M. Armand, H. Zhang, Z. Zhou, Taming the chemical instability of lithium hexafluorophosphate-based electrolyte with lithium fluorosulfonimide salts, Journal of Power Sources. 526 (2022) 231105. https://doi.org/10.1016/j.jpowsour.2022.231105.
[65] P. Handel, G. Fauler, K. Kapper, M. Schmuck, C. Stangl, R. Fischer, F. Uhlig, S. Koller, Thermal aging of electrolytes used in lithium-ion batteries – An investigation of the impact of protic impurities and different housing materials, Journal of Power Sources. 267 (2014) 255–259. https://doi.org/10.1016/j.jpowsour.2014.05.080.
[66] A.V. Plakhotnyk, L. Ernst, R. Schmutzler, Hydrolysis in the system LiPF6—propylene carbonate—dimethyl carbonate—H2O, Journal of Fluorine Chemistry. 126 (2005) 27–31. https://doi.org/10.1016/j.jfluchem.2004.09.027.
[67] H. Kim, S. Grugeon, G. Gachot, M. Armand, L. Sannier, S. Laruelle, Ethylene bis-carbonates as telltales of SEI and electrolyte health, role of carbonate type and new additives, Electrochimica Acta. 136 (2014) 157–165. https://doi.org/10.1016/j.electacta.2014.05.072.
[68] B.S. Parimalam, A.D. MacIntosh, R. Kadam, B.L. Lucht, Decomposition Reactions of Anode Solid Electrolyte Interphase (SEI) Components with $LiPF_6$, The Journal of Physical Chemistry C. 121 (2017) 22733–22738. https://doi.org/10.1021/acs.jpcc.7b08433.
[69] B. Lestriez, S. Bahri, I. Sandu, L. Roué, D. Guyomard, On the binding mechanism of CMC in Si negative electrodes for Li-ion batteries, Electrochemistry Communications. 9 (2007) 2801–2806. https://doi.org/10.1016/j.elecom.2007.10.001.

[70] W. Zhao, G. Zheng, M. Lin, W. Zhao, D. Li, X. Guan, Y. Ji, G.F. Ortiz, Y. Yang, Toward a stable solid-electrolyte-interfaces on nickel-rich cathodes: LiPO2F2 salt-type additive and its working mechanism for LiNi0.5Mn0.25Co0.25O2 cathodes, Journal of Power Sources. 380 (2018) 149–157. https://doi.org/10.1016/j.jpowsour.2018.01.041.
[71] I.A.J. Gordon, S. Grugeon, H. Takenouti, B. Tribollet, M. Armand, C. Davoisne, A. Débart, S. Laruelle, Electrochemical Impedance Spectroscopy response study of a commercial graphite-based negative electrode for Li-ion batteries as function of the cell state of charge and ageing, Electrochimica Acta. 223 (2017) 63–73. https://doi.org/10.1016/j.electacta.2016.12.013.
[72] Y. Cui, S. Xu, High tap density of Ni3(PO4)2 coated LiNi1/3Co1/3Mn1/3O2 with enhanced cycling performance at high cut-off voltage, Chinese Journal of Chemical Engineering. 23 (2015) 315–320. https://doi.org/10.1016/j.cjche.2014.03.001.
[73] D.-J. Lee, B. Scrosati, Y.-K. Sun, Ni3(PO4)2-coated Li[Ni0.8Co0.15Al0.05]O2 lithium battery electrode with improved cycling performance at 55°C, Journal of Power Sources. 196 (2011) 7742–7746. https://doi.org/10.1016/j.jpowsour.2011.04.007.
[74] M.F.A. Dove, R.C. Hibbert, N. Logan, Difluorophosphate Complexes of Chromium, Manganese, Iron, Cobalt, and Nickel t, J. CHEM. SOC. DALTON TRANS. (1985) 4.
[75] C.M. Mikulski, L.L. Pytlewski, N.M. Karayannis, Reactions between Triethyl Phosphate and Metal Halides, Z. Anorg. Allg. Chem. 403 (1974) 200–210. https://doi.org/10.1002/zaac.19744030216.

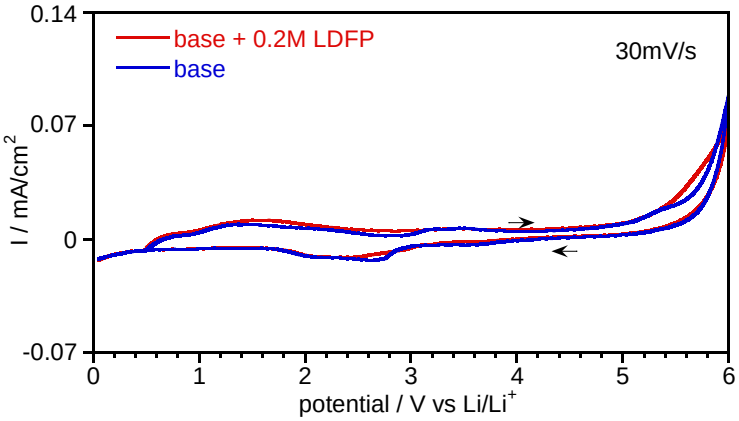

Figure 1 Cyclic voltammetry of both electrolytes using platinum as working and counter electrodes, and Li as reference electrode, at a scan rate of 30 $mV.s^{-1}$.

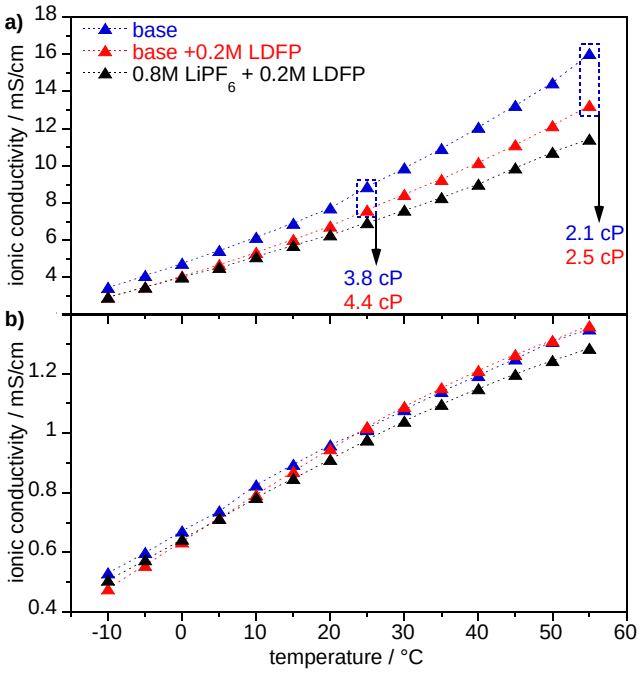

Figure 2. Ionic conductivity measurements performed in **a)** liquid and **b)** liquid impregnated in a porous polypropylene separator (Celgard 2500). Dashed rectangles in **a)** correspond to viscosity measurements.

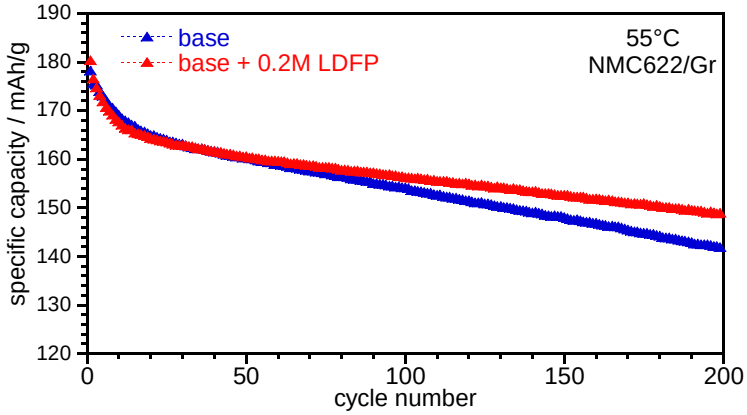

Figure 3. Capacity retention of 622/graphite pouch cells cycled between 2.8 – 4.3 V at C/4 (calculated for a total delithiation) and at 55°C without or with 0.2M LDFP.

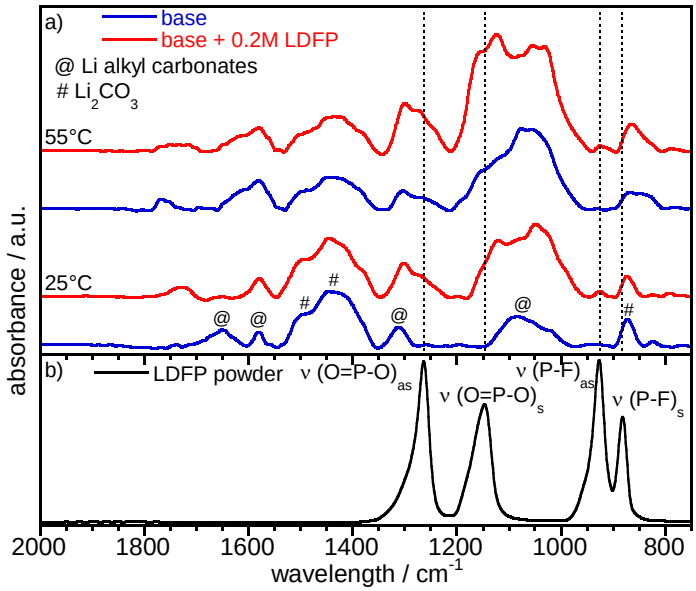

Figure 4. FT-IR analyses in the transmission mode of **a)** the SEI formed on graphite composite powders after one cycle in a half cell, between 1.5 - 0.01 V, at 25°C and 55°C without/with 0.2 M of LDFP, at C/20 and **b)** LDFP reference.

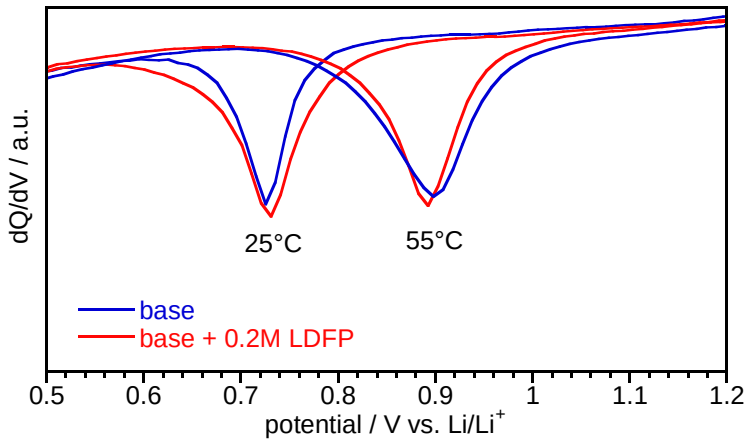

Figure 5. dQ/dV derivative curves showing the SEI formation potential range during the first lithiation of a graphite composite powder in half cell.

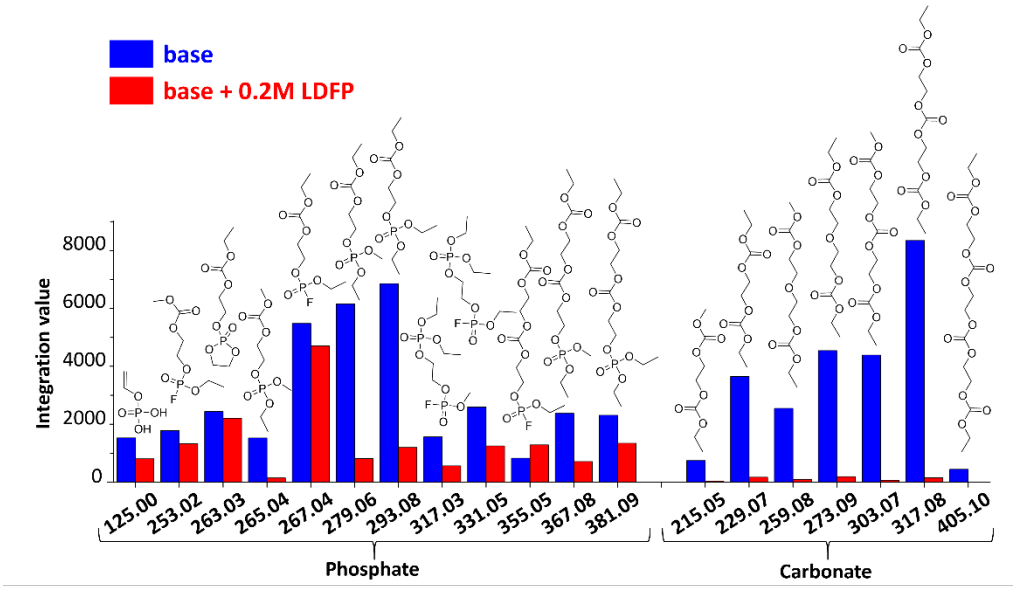

Figure 6. Phosphate and carbonate compounds analyzed by UHPLC-ESI-HRMS in electrolyte after 34 cycles (20 days) with base and base + 0.2M LDFP electrolytes. All peaks correspond to Na^+ adduct.

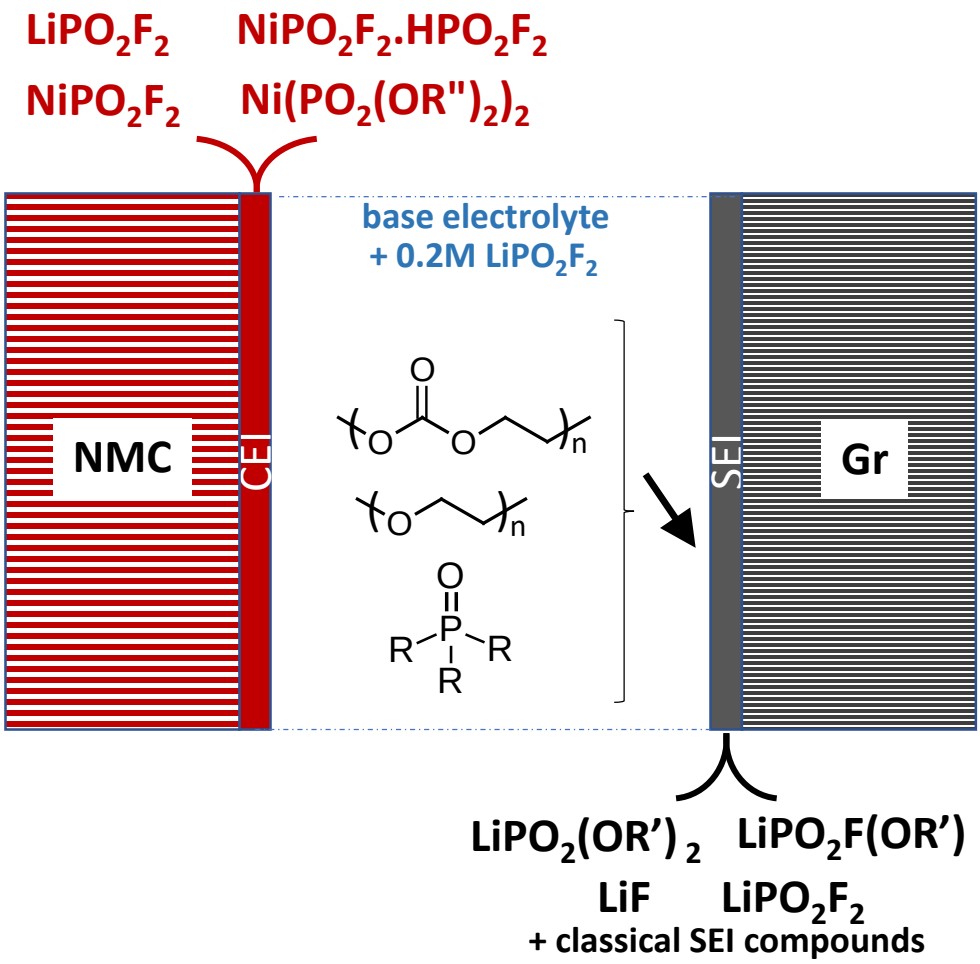

Figure 7. Scheme of the proposed LDFP impact on interphases and electrolyte composition. R = F, alkoxide, carbonate, phosphate; R' = Me, Et, $OC_2H_4OCO_2CH_3$, $OC_2H_4OCO_2C_2H_5$; R" = Me, Et.